Proteasome-dependent degradation of histone H1 subtypes is mediated by its C-terminal domain.

Authors: García-Gomis D[1], López J[1], Andrés M[1], Ponte I[1], Roque A[1]*.

Affiliation: [1]Biochemistry and Molecular Biology Department, Biosciences Faculty. Universitat Autònoma de Barcelona, Spain.

*Corresponding author

Keywords: histone H1, 20S proteasome, intrinsically disordered domains, phosphorylation

Abstract

Histone H1 is involved in chromatin compaction and dynamics. In human cells, the H1 complement is formed by different amounts of somatic H1 subtypes, H1.0-H1.5 and H1X. The amount of each variant depends on the cell type, the cell cycle phase, and the time of development and can be altered in disease. However, the mechanisms regulating H1 protein levels have not been described. We have analyzed the contribution of the proteasome to the degradation of H1 variants in human cells using two different inhibitors, MG132 and bortezomib. H1 variants accumulate upon treatment with both drugs indicating the role of the proteasome in the regulation of H1 protein levels. The global increase in histone H1 caused slight changes in chromatin as the excess is accumulated in the cytoplasm, presumably to prevent alterations in the nuclear processes. We analyzed the pathway of H1 degradation by the proteasome. Our results suggest that H1 degradation is ubiquitin-independent, whereas the whole protein and its C-terminal domain can be degraded by 20S proteasome. Our findings revealed a new regulatory mechanism for histone H1 degradation, where its basicity and intrinsically disordered domains are responsible for its targeting and degradation by the 20S proteasome.

Introduction

Histone H1 is a multigene family associated with the regulation of chromatin structure. In humans, the H1 family is composed of eleven subtypes or variants. Seven subtypes (H1.0-H1.5, H1X) are differentially expressed in somatic cells, while the remaining four are germ-line specific (Talbert et al. 2012). Somatic subtypes are subdivided into two groups: replication-dependent (RD) and replication-independent (RI). The expression of the RD subtypes (H1.1-H1.5) is associated with that of core histones, increasing during the S-phase and decreasing sharply in G2/M (Duronio and Marzluff, 2017). The RI subtypes, H1.0 and H1X, have different expression patterns during the cell cycle (Millán-Ariño et al., 2016).

Histone H1 subtypes are basic proteins with three structural domains: the N-terminal domain (NTD), the globular domain (GD), and the C-terminal domain (CTD). The globular domain has approximately 80 residues and a stable fold containing a winged-helix motif (Ramakrishnan et al., 1993; Cerf et al., 1993). This domain is responsible for H1 binding to the nucleosome dyad and it is highly conserved in evolution (Ramakrishnan et al., 1993; Ponte et al., 1998). The NTD is a short domain of 20-36 residues, while the CTD is the longest domain with about 100 residues. Both terminal domains are intrinsically disordered regions enriched in proline, serine, alanine, and especially lysine (Vila et al., 2001, Vila et al., 2002; Roque et al., 2005, Hansen et al., 2006). The CTD is the main determinant of chromatin compaction within histone H1 (Hendzel et al., 2004). This domain contains several cyclin-dependent kinases (CDK) consensus sites, which are modified in a cell cycle-dependent manner and affect the secondary structure of the CTD bound to DNA and chromatin, as well as the residence time of H1 in chromatin and its compaction (Roque et al., 2008; Raghuram et al., 2013; Lopez et al., 2015). H1 phosphorylation also facilitates nuclear export (Bleher and Martin, 1999).

The protein levels of histone H1 are tightly regulated during development as they can alter chromatin compaction and transcription. In stem cells, there is approximately one H1 molecule in every two nucleosomes (H1: nucleosome ratio of 0.5) (Fan et al., 2005). This ratio results in a chromatin structure characterized by its accessibility and high transcriptional activity (Zhang et al., 2012). In adults, the H1: nucleosome ratio increases, with values between 0.8 and 1 (Pan and Fan, 2016). In cells with very low transcriptional activity, like chicken erythrocytes, this ratio increases up to 1.3, promoting gene silencing (Bates and Thomas, 1981; Delcuve and Davie, 1989; Beacon and Davie, 2021). Gene knockout or knockdown affecting one or two H1 subtypes is not lethal, as the loss is compensated by increasing the levels of other subtypes, usually H1.0 (Fan et al., 2003; Izquierdo-Bouldstridge et al., 2017). However, triple knockout of H1.2, H1.3, and H1.4 in mice is deleterious during gestation, and the embryonic stem cells derived from these embryos had alterations in the nucleosome spacing and impaired differentiation (Fan et al., 2003; Zhang et al., 2012). Therefore, it is interesting to study which are the regulatory mechanisms that control H1 protein levels.

Proteolysis is a crucial regulatory mechanism in the maintenance of proteostasis. Three mechanisms contribute to protein degradation: proteases, the lysosomal system, and the proteasome complex. Proteasomal degradation is responsible for the elimination of most damaged, misfolded, or unfolded proteins in the cell. Proteasomes are located in the nucleus and in the cytoplasm (Peters et al., 2004). The proteolytic activity is within a barrel-shaped protein

complex known as the 20S proteasome or core particle. The 20S proteasome is formed by four stacked heptameric rings. The external rings contain seven α subunits, while the internal rings contain seven β subunits. The catalytic subunits, β1, β2, and β5 have post-glutamyl, trypsin-like, and chymotrypsin-like activities, respectively. The 20S proteasome can associate with different regulatory particles or lids on one or both ends (Fricker, 2020).

There are two pathways of proteasomal degradation of proteins: ubiquitin (Ub)-dependent and Ub-independent. Protein degradation is mediated by the 26S proteasome formed by the 20S proteasome and the 19S regulatory particle. The targeting of substrates involves the addition of one or more ubiquitin monomers (Shabek et al., 2012). Proteins degraded by the Ub-independent proteasomal pathway are recognized by different signals, such as specific amino acid sequences (Murakami et al., 1992), post-translational modifications (Qian et al., 2013), or regions enriched in basic and flexible amino acids (Kudriaeva et al., 2019). Degradation is carried out directly by the 20S proteasome or coupled with PA28 or PA200 regulatory particles.

Core histones are long-lived proteins, but their degradation is triggered under specific conditions, such as response to EGF, DNA damage, and oxidative stress (reviewed in Dhaenens et al., 2015; Shmueli et al., 2022). In contrast, the proteolytic mechanisms involved in the regulation of histone H1 protein levels are largely unexplored. Early studies showed that the turnover rate of histone H1 is higher than that of core histones, and its magnitude is variable depending on the replicative state of the cells. H1 half-live in rat brain changed from 13 to 112 days between neonate and adult animals, while its value decreased to hours in K562 cells in culture (Duerre and Lee, 1974; Ullrich and Grune, 2001). The degradation rate of histone H1 was enhanced after exposure to oxidative conditions by the action of the 20S proteasome. In these conditions, activation of PARP1 accelerated H1 degradation (Ullrich and Grune, 2001). Induction of glycoxidation with glyoxal promoted H1 degradation by the nuclear proteasome (Cervantes-Laurean et al., 2005). Histone H1 proteolysis is also enhanced by gamma-irradiation and TNF-induced apoptosis (Voelkel-Johnson et al., 1995; McConkey, 1996).

In the present work, we have studied the contribution of the proteasome to the regulation of histone H1 protein levels. Using proteasome inhibitors, we have analyzed the accumulation of H1 subtypes, the changes in subcellular distribution, and the effect on chromatin. We have also examined the pathway of proteasomal degradation and the contribution of histone H1 structural domains.

Materials and methods

Cell culture and treatments.

All the cell lines were grown at 37°C and 5%CO2 in their specific culture media supplemented with 10% fetal calf serum (Gibco) and 1% penicillin-streptomycin (Ddbiolab). Human embryonic kidney 293T cells (HEK293T) and cervical carcinoma cells (HeLa) were cultured in DMEM Glutamax (Corning). For human breast cancer cells (T47D), the culture media was RPMI (Corning), supplemented with 2 mM L-glutamine (Ddbiolab). After harvesting, cells were counted in an automated cell counter (Bio-Rad). For proteasome inhibition, cells were treated with 20 µM MG132 (Sigma) or 20 nM bortezomib (BTZ) (Labnet) for 12 h. Both drugs were dissolved in dimethyl sulfoxide (DMSO). The same amount of DMSO was added to untreated cells as a negative control. Proteasome inhibition was confirmed by fluorimetry, and the effect on the protein levels was analyzed by Western blot. Protein stability was analyzed by translation inhibition with 10 µg/mL cycloheximide (Sigma) for 8 h. Then, cells were harvested, proteins extracted, and analyzed by Western blot.

Analysis of proteasomal activity.

Proteasome inhibition was assessed by measuring the chymotrypsin-like activity using the fluorogenic peptide, Suc-LLVY-AMC, as described by Zafar et al., 2007. Half a million cells were resuspended in 50 mM Tris HCl buffer (pH 7.8) containing 0.25 % of NP-40, 0.5 mM dithiothreitol, 5 mM $MgCl_2$, and 2 mM ATP. The cell suspension was incubated at room temperature for 30 minutes. Then, 200 µM of Suc-LLVY-AMC were added and the digestion was allowed to proceed for 1h at 37 °C. The reaction was stopped by the addition of ice-cold ethanol and the samples were centrifuged for 10 minutes at 10000 g. The supernatant was assayed for release of the fluorophore, 7-amino-4-methylcoumarin. Fluorescence scans were recorded in a Varian Cary Eclipse fluorimeter using the following parameters: excitation wavelength, 345 nm, and emission wavelength interval, 360-500 nm. As a positive control, Suc-LLVY-AMC was digested *in vitro* with 1 unit of chymotrypsin for 15 minutes at 37 °C. The chymotrypsin activity was calculated using the fluorescence values at 438 nm and expressed as a percentage of the Suc-LLVY-AMC digested *in vitro.*

Preparation of total protein extracts.

Cells were harvested by trypsinization and washed twice with PBS. Cells were resuspended in a 50 mM Tris pH 8 buffer containing 300 mM NaCl, 1 % Triton X-100, 0.5 % sodium deoxycholate, 3 mM DTT, and a protease inhibitor cocktail (PIC), and incubated for 30 minutes on ice. The cell suspension was passed through a needle until it was homogeneous, and the cell lysate was centrifugated at 16000 g, 30 minutes, at 4 °C. Protein concentration was determined with Bradford.

Western blot.

Equivalent amounts of total proteins (10 µg) were separated in a 12% denaturing polyacrylamide gel electrophoresis (SDS-PAGE) and electrotransferred to a polyvinylidene difluoride membrane (PVDF) (EMD Millipore) at 100 V for 1 h. Immunoblot analyses were performed with the conditions recommended by the manufacturer for each antibody: anti-H1.0 (Merck, 05-629-I); anti-H1.2

(Thermofisher, 711909); anti-H1.3 (Abcam, ab183736); anti-H1.4 (Thermofisher, 702876); anti-H1.5 (Thermofisher, 711912); anti-H1X (Abcam, ab31972); anti-β-catenin (BD Transduction Laboratories™, 610153); anti-α-tubulin (Fisher scientific, 11839933); anti-Histone H3 (Abcam, ab1791). The excess of primary antibodies was washed with TBS-0.1 % Tween, three times. The membranes were incubated with mouse or rabbit secondary antibodies (Bio-Rad), according to the manufacturer's instructions for 1 h at room temperature. Membranes were washed three times with TBS, and the blots were visualized with Clarity Western ECL substrate (Bio-Rad) in a Chemidoc imaging system (Bio-Rad). The intensities of immunoreactive proteins were quantified using Image Lab software (Bio-Rad). The blots were probed with α-tubulin as a loading control.

Quantification of mRNA levels by RT-qPCR.

The levels of mRNA of histone H1 subtypes were analyzed by RT-qPCR. Total RNA was purified from one million cells with the High Pure RNA Isolation kit (Roche) following the manufacturer's instructions. Purified RNA was quantified by Nanodrop (Thermo Scientific), and 100 ng were retrotranscribed with iScriptTM cDNA synthesis kit (Bio-Rad) using random hexamers as primers. Next, H1 subtypes were amplified by qPCR using primers specific for each H1 subtype (Table S1). The reaction mixture contained 1 ng of cDNA, 0.5 µM of each primer, and SYBR supermix (BioRad) in a final volume of 20 µL. The cycle parameters were as follows: one cycle of 95 °C for 3 min, 40 cycles of 95 °C for 10 s, and 60 °C for 30 s, followed by the melting curve (65 °C-95 °C). Negative controls without retrotranscriptase were included in every assay for each gene. Each sample was analyzed in triplicate. Mean Cqs were calculated for all H1 subtypes and GAPDH, the housekeeping gene used as a control. Triplicates with a difference in Cq values > 0.5 cycles were rejected. Fold change was calculated using the ddCT method (Livak and Schmittgen, 2001).

Immunofluorescence.

Cells were grown on the desired conditions, counted, and diluted in PBS to a final concentration of $5 \cdot 10^4$ cells/mL. 500 µL were spun down for 10 min at 500 g in a Thermo Shandon Cytospin 3 using a single-chamber Cytospin funnel as described by Izquierdo-Bouldstridge et al., 2017. Cells were air-dried for 1 h at room temperature and then fixed with 2 % paraformaldehyde at room temperature for 10 min. Fixed cells were permeabilized with PBS-0.5 % Triton X-100 and blocked with PBS 0.1 % Tween, 2 % bovine serum albumin for 1 h at room temperature. For immunodetection, primary antibodies were incubated at 4 °C overnight and secondary antibodies at room temperature for 1 h. Antibodies against H1.4-T146p (Abcam, ab3596), hyperphosphorylated H1 (Merck, 06-597), and H1 subtypes (described previously) were used. Secondary antibodies were all Alexa-488 conjugated from Invitrogen (A11034 and A11017, dilution 1:500). Images were taken using Leica SP5 AOBS confocal microscope. Nuclei were stained with DAPI (0.1 µg/ml). Quantification of the nuclear and cytoplasmatic fluorescence was carried out using the microscopy imaging software Imaris (Oxford instruments). The amount of H1 in the cytoplasm was determined as the difference between total cellular fluorescence and the fluorescence within the nuclear surface in the fluorescence channel corresponding to H1 subtypes. The nuclear surface was determined using DAPI as a marker. The values were expressed as a percentage of the total fluorescence. For each condition and subtype, 35 to 70 cells were analyzed. The Kolmogorov-Smirnov test was used to determine whether the percentage values followed a normal distribution. The effect of the treatment on the proportion of cytoplasmatic H1

was assessed with the Student's T-test. All the statistical analyses were performed at https://www.socscistatistics.com/.

Chromatin extraction.

To study H1 subtypes bound to chromatin in untreated cells and after treatment with MG132, chromatin fragments were prepared by sonication. Cells were fixed using 1% formaldehyde, harvested, and sonicated in a Bioruptor (Diagenode) to generate chromatin fragments between 200 and 500 bp. The cross-linking was reversed by incubation at 65°C overnight, and the proteins were analyzed by Western blot.

Nuclease accessibility assay.

Harvested cells were washed three times in PBS and resuspended in a hypotonic buffer containing 10 mM HEPES pH 7.9, 1.5 mM $MgCl_2$, 10 mM KCl, 0.1 mM PMSF and PIC. The suspension was incubated at 4°C for 30 minutes in an orbital shaker and centrifuged at 800 g for 5 minutes. The nuclear pellet was washed in a buffer containing 10 mM Tris pH 7.4, 3 mM $MgCl_2$, 60 mM KCl, and 1 % thiodiglycol, centrifuged at 800 g for 5 minutes, and resuspended in the same buffer to a final DNA concentration of 1 mg/mL. Chromatin digestion was performed by adding 0.5 mM CaCl2 and micrococcal nuclease (Sigma) at a concentration of 1U/50 µg of DNA. The digestion was allowed to proceed at 37°C, and aliquots were taken at different times. In all cases, the digestion was stopped by the addition of EDTA to a final concentration of 10 mM. Nuclei were sedimented at 4500 g for 5 minutes and lysed in TE buffer pH 8.0 for 30 minutes at 4°C. Soluble chromatin was obtained after centrifugation at 16000 g for 10 minutes. The supernatant was placed in a clean tube, and the proteins were digested with 100 µg/mL proteinase K (Sigma) at 37°C overnight. DNA fragments were extracted with phenol-chloroform-isoamyl alcohol (25:24:1) and precipitated with two volumes of absolute ethanol at -20°C. The DNA fragments were separated by electrophoresis in a 1.5 % agarose gel, stained in 10 µg/mL ethidium bromide, and visualized in GeldocXR (Bio-Rad).

Sulfuric acid extraction of histones.

The extraction of histones with sulfuric acid was performed using whole cells or the nuclear fraction. Harvested cells were washed in PBS. The cell pellets were resuspended in 0.2 M sulphuric acid. The suspension was incubated for 1 h at 4 °C in an orbital shaker and centrifuged at 16000 g for 15 min at 4 °C. The supernatant containing the soluble histones was kept. The chromatin pellet was re-extracted for 30 min more using the same procedure. The supernatants were pooled and histones were precipitated for 2h at 4 °C with 20% (w/v) TCA. Next, the samples were centrifuged at 16000 ×g for 15 min at 4 °C. The protein pellets were washed three times with acetone and dried at room temperature. Extracted H1s were resuspended in MilliQ distilled water and quantified by absorbance at 210 nm. Nuclear fraction was obtained as described in the perchloric extraction protocol. This fraction was processed as described above for whole cells. The protein extracts were analyzed by 12-15% SDS-PAGE and stained with 0.1% Coomassie blue. Images were taken using a Chemidoc imaging system (Bio-Rad).

Analysis of ubiquitinated proteins.

Transfection of HEK-293T cells with pHis-Ubiquitin (Addgene, 31815) was performed by the calcium phosphate-DNA precipitation method (Kwon and Firestein, 2013). After 48 h, cells were treated with MG132, harvested, and total protein extracts were prepared as described above. Ubiquitinated proteins were immunoprecipitated using magnetic Protein A Dynabeads (Thermofisher) loaded with an antibody against His-tagged proteins (Finetest, FNab00008). Immunoprecipitation was carried out overnight, at 4 °C, in 20 mM Tris pH 7.5, 150 mM NaCl, 1 mM EDTA, 1 mM EGTA, 1 % Triton X-100, and (PIC) (Thermofisher). Beads were washed three times, and proteins were eluted in 2x SDS sample buffer at 95°C for 10 min. The presence of ubiquitinated H1s was analyzed by Western blot, using β-catenin as a positive control.

Perchloric acid extraction of histone H1 subtypes.

Harvested cells were washed in PBS and resuspended in a hypotonic buffer containing 10 mM HEPES pH 7.9, 1.5 mM MgCl2, 10 mM KCl, 0.1 mM PMSF, and PIC. The suspension was incubated at 4°C for 30 minutes in an orbital shaker and centrifuged at 800 g for 5 minutes. HClO4 at a final concentration of 5% (w/v) was added to the nuclear fraction and incubated for 1 h mixing in an orbital shaker at 4 °C. The suspension was centrifuged at 16000 ×g for 15 min at 4 °C. The supernatant containing the soluble H1s was kept. The chromatin pellet was re-extracted for 30 min more using the same procedure. The supernatants were pooled, and H1s were precipitated overnight at 4 °C with 20% (w/v) TCA. Next, the suspension was centrifuged at 16000 ×g for 15 min at 4 °C. The protein pellets were washed three times with acetone and dried at room temperature. Extracted H1s were resuspended in MilliQ distilled water and quantified by absorbance at 210 nm.

Preparation of recombinant proteins.

Recombinant proteins corresponding to H1.0, as well as its globular domain (GD) and C-terminal domain (CTD), were expressed and purified from *Escherichia coli (E. coli)*. The recombinant plasmids pH1.0 and pCTDH1.0 were transformed into *E. coli* M15 cells, while pGDH1.0 was transformed into *E. coli* BL21(DE3). Cells were grown to an OD_{600nm} of 0.8 and then induced with 1 mM IPTG, allowing expression to proceed for 4 h at 37°C. Cells were then harvested and stored at -80°C. Recombinant H1.0 and the CTD were purified by metal-affinity chromatography and desalted by gel filtration, as previously described (Roque et al., 2004). The GD was purified according to the protocol described for the globular domain of chicken histone H5 (Goytosolo et al., 1996).

***In vitro* digestion with the 20S proteasome.**

We analyzed the degradation kinetics of 200 ng/condition of recombinant H1.0, CH1.0, and GH1.0, and 1 µg/condition of the perchloric acid purified histone mixture from T47D cells, using the protocol described by Kudriaeva et al., 2019. Bovine serum albumin (Sigma) was used as a negative control. Proteolytic digestion was performed in 20 mM Tris pH 7,5, 20 mM NaCl, 1 mM EDTA, and 1 mM DTT, in the presence of 5 nM of 20S proteasome (Boston Biochem, E-360), at 37 °C. The reaction was stopped by adding electrophoresis loading buffer and incubating the samples at 95 °C for 5 minutes. The digestion products were analyzed by 12-15 % SDS-PAGE and stained

with Coomassie blue or silver (Silver stain plus kit, Bio-rad). Images were taken using a Chemidoc imaging system (Bio-Rad). Degradation intermediates were further characterized by top-down mass spectrometry.

Mass spectrometry analysis.

Top-down mass spectrometry was performed at the IRB Barcelona Mass Spectrometry and Proteomics Core Facility, which is a member of ProteoRed, PRB3-ISCIII, supported by grant PRB3 (IPT17/0019 - I SCIII-SGEFI / ERDF) and is granted in the framework of the 2014-2020 ERDF Operational Programme in Catalonia, co-financed by the European Regional Development Fund (ERDF). Reference: I U16-015983. Briefly, degradation intermediates of H1.0 digested with proteasome 20S *in vitro* were analyzed by top-down proteomics. The sample was cleaned-up using C4-tips (polyLC) and separated by nanoLC with an Acquity UPLC M-Class BioResolve mAb Column (Waters). Proteoforms were eluted using a combination of two eluents: A. H_2O 0.1 % formic acid; B. CH_3CN 0.1 % formic acid in the following proportions: 10 % to 50 % of B in 120 min + 50 % to 85 % in 7 min. The chromatography was performed at a flow rate of 300 nL/min at 60°C. The sample was ionized by nESI, using Advion Triversa Nanomate (Advion BioSciences) as a source at 1.7 kV, 0.5 psi, in a positive mode. MS/MS was performed in an Orbitrap Fusion Lumos™ Tribrid (Thermo Scientific) in a data-dependent mode. The ions were fragmented by ETD, with 10% supplemental energy from HCD. Proteoform identification was performed using Top-Down PSCW database creation from XML inside Proteome Discoverer software (v2.5) (Thermo Scientific). BioPharma Finder v4.0 (Thermo Fisher Scientific) was used to extract averaged mass spectra from detected chromatographic peaks (MS1). Deconvolution was done using the auto Xtract algorithm on resolved m/z charged species. The slice window option was set to a target average spectrum width of 0.1 min. The recombinant H1.0 sequence was introduced to find a match between the experimental and theoretical masses.

Results

Effect of proteasome inhibitors in the protein levels of H1 subtypes.

We analyzed the role of the proteasome in the control of the protein levels of histone H1 subtypes by inhibition experiments. The proteasome inhibition was assessed using the peptide Suc-LLVY-AMC, which releases the fluorophore after digestion by the chymotrypsin-like activity of the proteasome (Zafar et al., 2007). The results showed that treatment with MG132 inhibited proteasome activity at the selected dose (Figure S1).

The effect on the protein levels was analyzed by Western blot. Treatment with MG132 caused an accumulation of β-catenin, a known proteasomal substrate, which was used as a positive control of the treatment (Aberle et al., 1997). We observed an accumulation of all the expressed H1 subtypes in T47D and HeLa (Figures 1A and S2). All H1 subtypes, except H1.1, are detectable in T47D by Western blot (Figure 1A). We observed differences in the accumulation of somatic H1 subtypes (Figure 1B). The subtype with the highest increase in protein levels was H1.0, followed by H1X and H1.4. Subtypes H1.2, H1.3, and H1.5 also accumulated but to a lesser extent. In HeLa, four subtypes were readily detectable by Western blot, H1.2, H1.4, H1.5, and H1X, while H1.0 was detected as a very faint band. As we observed in T47D, all H1s accumulated after treatment with MG132 (Figure S2). In HeLa, as in T47D, H1.0 was the subtype with the highest accumulation, followed by H1X and H1.4.

MG132 inhibits the proteolytic activity of the proteasome and calpains, so we also used bortezomib (BTZ), a specific proteasome inhibitor (Goldberg AL, 2012; Fricker LD, 2020). In the presence of bortezomib, all H1 subtypes accumulated, confirming the role of the proteasome in regulating H1 protein levels (Figure 1A). The level accumulation of H1 subtypes was slightly lower than in MG132, except for H1.2. These results suggested that other proteolytic mechanisms might contribute to the degradation of H1 subtypes.

The distinct accumulation of H1 subtypes upon proteasome inhibition may be explained by differences in protein stability. Therefore, we inhibited protein synthesis with cycloheximide and analyzed the remaining protein of each subtype by Western blot (Figures 1C and 1D, Figures S3A and S3B). In T47D, inhibition of protein translation caused a decrease in the protein levels of H1 subtypes, albeit in different proportions. The highest decrease was observed in H1.0, the subtype with the highest accumulation in MG132. The protein accumulation of H1 subtypes upon proteasome inhibition with MG132 had a negative correlation ($r = -0.96$) with the protein fraction remaining after translation inhibition with cycloheximide (Figure 1E). In HeLa, we observed a similar correlation between the accumulation of H1 subtypes and their stability ($r = -0.99$) (Figure S3C). In this cell line, H1.0 was also the subtype with the highest accumulation, but its stability could not be measured due to the low levels present at the initial conditions. Our results suggest that H1 subtypes with a higher protein accumulation are less stable, so their protein levels depend on their translation rate.

Protein accumulation may be modulated at the transcript level, so we analyzed the effect of proteasome inhibition in the mRNA levels of H1 subtypes. Treatment with MG132 caused a decrease in the transcript levels of all H1 subtypes in HeLa and T47D (Figure S4). Subtypes H1.0 and H1X were reduced to less than 60 % of the untreated values, while in the replication-

dependent subtypes, mRNA levels were reduced to less than 30 %. The more apparent effect of the proteasome inhibition in the transcript levels of the replication-dependent subtypes led us to analyze whether the cell cycle was affected by the treatment with MG132. We found no significant changes in the proportions of cell cycle phases in T47D upon proteasome inhibition (Figure S5). Two main causes could explain the changes described above: i) a feedback regulatory loop triggered by the increase in the protein levels, and ii) indirect effects of the drug.

Distribution of H1 subtypes after proteasome inhibition.

The increase in the protein levels of H1 subtypes upon proteasome inhibition could have an impact on their subcellular distribution. We analyzed the changes in H1 subtypes by immunofluorescence. Histone H1 is mainly a nuclear protein, but its presence in the cytoplasm could be detected by immunofluorescence (Zlatanova et al.,1990).

The levels detected in the cytoplasm of T47D cells differed depending on the subtype. The percentages of cytoplasmatic H1.0 and H1.5 were less than 10%, approximately 10% for H1.3 and H1.4, and more than 15% for H1.2 and H1X (Figure 2). After treatment with MG132, the amount of all H1 subtypes increased in the cytoplasm, in particular for H1.5 (Figure 2). The increase was statistically significant, except for H1.3. Histone H3 was also detected in the cytoplasm, but at a similar level in both conditions, indicating that the increase in H1 was not due to altered permeabilization of the nuclear membrane or the disruption of chromatin structure. The accumulation in the cytoplasm was observed for all subtypes in T47D cells treated with BTZ (Figure S6) and in H1.2 in HeLa treated with MG132 (Figure S7). The increase was statistically significant, except for H1.0 and H1X in BTZ (Figures S6 and S7).

The presence of post-translational modifications, in particular phosphorylation, can alter H1 affinity for chromatin, as well as its subcellular localization (Bleher and Martin, 1999; Bolton et al., 1999). We used two antibodies against phosphorylated H1 to analyze if there were changes in its subcellular distribution upon proteasome inhibition (Figure 3A). The first antibody is against H1 from Tetrahymena and recognizes hyperphosphorylated H1. The second antibody recognizes H1.4T146p, a CDK2 consensus site present in H1.2 and H1.3. The percentages of phosphorylated H1 in the cytoplasm were higher than 15% and comparable in magnitude to the more abundant subtypes in the cytoplasm. The addition of MG132 caused a significant increase in the cytoplasmic levels of phosphorylated H1 (Figure 3B). Hyperphosphorylated H1 remained dispersed in the nucleus and the cytoplasm, while the nuclear foci observed with the H1.4T146p antibody were more abundant and intense in the presence of MG132. The relative increase of both types of phosphorylation suggests that this modification could contribute to the accumulation of H1 in the cytoplasm, although it may not be the only cause.

Effects of proteasome inhibition in chromatin.

The accumulation of H1 subtypes may alter chromatin structure and compaction. We analyzed the changes in the H1 bound to chromatin after proteasome inhibition by analyzing DNA-crosslinked H1 using Western blot (Figures 4A and 4B). The treatment with MG132 caused a rearrangement in the proportion of the subtypes bound to chromatin. The amount of H1.0 and H1.2 bound to chromatin increased, while that of H1.4 and H1.5 decreased. Subtypes H1.3 and H1X remained unaltered.

To analyze the impact of H1 accumulation on chromatin compaction we determined the H1: nucleosome ratio using sulfuric acid extractions of the isolated nuclei and whole cells. We found that the ratio H1: nucleosome increased 1.5-fold in the whole cell extract, while in the nucleus it was 0.96-fold, almost identical to the untreated (Figures 4C and 4D). These findings confirmed the increase in the cytoplasm observed by immunofluorescence. We analyzed if there were changes in chromatin accessibility after proteasome inhibition with MG132 by digestion with micrococcal nuclease. The digestion pattern was similar between the two samples, although a slight increase in accessibility could be observed (Figure 4E). However, the nucleosome repeat length (NRL) remained unaltered (Figure 4F). These results suggest that the accumulation of H1 in the cytoplasm after proteasome inhibition prevents significant changes in chromatin structure and compaction.

Mechanism of degradation of histone H1 subtypes by the proteasome.

Protein degradation by the proteasome can occur through different pathways. The most common one is the degradation of ubiquitinated proteins by 26S proteasome. Protein mono- or polyubiquitination causes an increase in the molecular weight of the targeted proteins. In the case of H1, we detected an accumulation of all subtypes after treatment with proteasome inhibitors. However, the electrophoretic mobility of H1s remained unaltered, and no bands of higher molecular weight were observed, suggesting that the contribution of the ubiquitin-dependent proteasome degradation may not be its main degradation pathway.

To prove this hypothesis, we transfected HEK293T cells with a plasmid containing ubiquitin with a histidine tag. The expression of a His-tagged ubiquitin allowed the immunoprecipitation of ubiquitinated proteins, which could be detected by Western blot. First, we confirmed that H1 subtypes were accumulated in HEK293T cells upon proteasome inhibition. In this cell line, the H1 complement, characterized by Western blot, is composed of five subtypes: H1.0, H1.2-H1.4, and H1X. Like in T47D cells, all subtypes increased after treatment with MG132, with H1.0 and H1X being the ones more affected (Figure 5A and 5B).

After immunoprecipitating the protein extract with an antibody against the His-tag, we confirmed by Western blot the presence of ubiquitinated β-catenin in the cells treated with the inhibitor (Figure 5C). We also analyzed the replication-dependent subtypes expressed in HEK293T, which are usually more abundant than the replication-independent subtypes. Apparently, all three subtypes were immunoprecipitated due to unspecific interactions with the His-tag antibody, as the main band detected corresponded to the unmodified protein. We also detected a faint band of higher molecular weight in H1.3 and H1.4 that could correspond to ubiquitinated H1. This band was present in the untreated and treated cells showing little or no increase after treatment with MG132 (Figure 5C). These results suggest that the 26S proteasome is not the main pathway of H1 subtypes degradation.

Ubiquitin-independent proteasomal degradation can be performed by the 20S proteasome directly or in association with regulatory subunits PA200 or 11S (Fricker LD, 2020). The 20S proteasome can directly target basic proteins containing intrinsically disordered domains (Kudriaeva et al., 2019). Histone H1 is enriched in basic residues and contains two intrinsically disordered domains, so we analyzed whether the 20S proteasome catalyzed H1 degradation *in vitro*.

Using recombinant H1.0 as a model, we digested the whole protein and its structural domains with the 20S proteasome and analyzed the products by SDS-PAGE. The whole protein was readily digested, with the intact protein disappearing after 60 minutes and detecting lower molecular weight degradation intermediates (Figure 6A). These results suggested that H1 could be degraded directly by the 20S proteasome. The CTD intact band decreased with time, and products of lower molecular weight could be observed, showing similar behavior to the whole protein. In contrast, the GD and bovine serum albumin (BSA) used as a negative control remained stable throughout the reaction (Figure 6A). The NTD was not analyzed because even though it is also intrinsically disordered has only 20 residues, and therefore, it is not suitable for analysis with SDS-PAGE. The whole H1.0, as well as the CTD, is expressed with a histidine tag for purification. To discount the possibility that the tag could be involved in targeting the 20S proteasome, we digested *in vitro* a mixture of native H1s extracted with perchloric acid from T47D. We observed a similar pattern to that of recombinant H1.0, indicating that the degradation of the protein by the 20S proteasome was not associated with the histidine tag.

To further characterize the contribution of the individual domains of H1.0 to the degradation by the 20S proteasome, we analyzed the digestion intermediates by mass spectrometry (Figure 6B, Table S1). The top-down analysis detected 39 proteoforms of the digested protein with more than one protein-spectrum match (PSM). They could be divided into two groups. The first group had 23 proteoforms, 150 PSMs, and lacked the CTD. The second group was composed of 16 proteoforms with 42 PSMs, lacking the CTD and the NTD. These results indicate that the degradation of histone H1 by the 20S proteasome is determined by the intrinsically disordered properties of its CTD.

Discussion

We have examined the role of the proteasome in the control of histone H1 protein levels. Inhibition of the proteasome with MG132 caused the accumulation of all H1 subtypes in several human cell lines, indicating that it is involved in H1 proteolysis. We observed differences among H1 subtypes. The protein accumulation was higher in the less abundant H1 subtypes, H1.0 and H1X, suggesting that the differences could be determined, at least in part, by protein stability. We observed a negative correlation between H1 accumulation and protein stability, confirming our hypothesis. The replication-independent subtypes, in particular H1.0, had higher accumulation and were less stable. The regulation of these subtypes at the protein level allows for fast changes in the H1 complement in response to different stimuli. Experimental evidence has confirmed that H1.0 expression is regulated by external stimuli and that this subtype is a key player in the compensation of the H1 levels upon the knockdown of individual or multiple subtypes (Pan and Fan, 2016; Millán-Ariño et al., 2016; Izquierdo-Bouldstridge 2017; Di Liegro et al., 2018).

MG132 inhibits the proteasome and cellular proteases like calpains (Fricker LD, 2020). For that reason, we analyzed H1 accumulation in the presence of BTZ, a specific inhibitor of the proteasome (Goldberg et al., 2012; Kisselev et al., 2012; Fricker LD, 2020). We found that H1 accumulated less than in MG132, with some changes in specific subtypes. Two explanations, alone or together, could account for our findings: the differences between the two inhibitors and the action of other proteolytic mechanisms. Regarding the first possibility, MG132 at the doses used in our experiments inhibits all three catalytic activities in the proteasome (Bibo-Verdugo et al., 2017). Meanwhile, BTZ preferentially inhibits the chymotrypsin-like activity, to a lesser extent, the post-glutamyl activity, and does not inhibit the trypsin-like activity in the standard proteasome (Kisselev et al., 2012). Given that histone H1 is enriched in basic amino acids, the trypsin-like activity could be essential for its degradation, explaining some of the differences observed between the inhibitors. As for the second possibility, further experiments are needed to determine whether calpains are also involved in H1 degradation.

Upon proteasome inhibition, the transcript levels of H1 subtypes decreased. This difference was not associated with significant changes in the cell cycle in the presence of MG132. Although the indirect effects of the drug cannot be ruled out, our results open the possibility that transcriptional downregulation could also contribute to preventing the excess of H1 subtypes. The transcriptional regulation of H1 subtypes during the cell cycle and the evidence of co-transcriptional regulation are in favor of this feedback loop (Duronio and Marzluff, 2017; Ponte et al., 2021). This result suggests that the control of the protein levels of histone H1 is a process with multiple layers.

The multilayered regulation of H1 subtypes at the protein level could be necessary to protect the cell from the cytotoxic effect of its accumulation. An excess of histone H1 can result in its unspecific binding to chromatin, which can alter chromatin structure and transcription. Local alterations in chromatin structure, as well as in the transcript levels were observed in yeast after overexpression of core histones (Singh et al., 2010). In the case of histone H1, some biological systems, such as chicken erythrocytes confirm that a higher content of H1 in the nucleus promotes chromatin compaction and transcriptional silencing (Delcuve and Davie, 1989; Beacon and Davie, 2021). Inducible overexpression of recombinant H1.0 and H1.2 in mouse fibroblasts led to a reduction in the protein levels of the rest of the H1 subtypes while producing a moderate increase

in the H1: nucleosome ratio up to 1.3 when H1.0 was overexpressed (Brown et al., 1996). H1 overexpression reduced chromatin nuclease accessibility, increased nucleosome spacing, and caused alterations in gene expression (Gunjan et al., 1999; Bhan et al., 2008).

Histone H1 is mainly a nuclear protein, but a cytoplasmatic pool of H1 amounting to approximately 10% has been described (Zlatanova et al., 1990). Upon proteasome inhibition, we observed an increase in the cytoplasmatic pool of all H1 subtypes. The accumulation of histone H1 in the cytosol has been observed in mouse models of prion and Alzheimer's diseases (Bolton et al., 1999) and in response to the CDK inhibitor flavopiridol in primary CLL cells (Harshman et al., 2013). The preferential accumulation of histone H1 in the cytoplasm, maintaining the H1: nucleosome ratio almost constant in the nucleus, prevented global changes in chromatin structure, as observed in the nuclease accessibility assay. However, local alterations are still possible, as we detected rearrangements in the proportions of H1 subtypes bound to chromatin. Changes in the nuclear chromatin-bound H1 complement and the proportions of H1 subtypes in the cytoplasm could result from the combined effect of their differential characteristics, including protein stability, nuclear localization, chromatin affinity, and PTMs (Millán-Ariño et al., 2016; Andrés et al., 2021). In addition, the accumulation of H1 in the cytoplasm could cause unspecific binding to RNA molecules, potentially altering RNA-associated functions. The propensity of H1 to bind RNA molecules and promote phase separation has been recently reported, although its relevance in our conditions was not explored (Leicher et al., 2022).

It is known that phosphorylation of H1 promotes its accumulation in the cytoplasm (Bleher and Martin, 1999), so we tested if the amount of phosphorylated H1 was increased in this compartment by immunofluorescence using two different antibodies. We found a slight increase in phosphorylated H1 in the cytoplasm, suggesting that this modification could contribute to its accumulation in this compartment. The extent of the contribution of phosphorylation could be higher than the one we observed, considering that the available antibodies didn't target directly phosphorylated positions in H1.5, the subtype with the greatest increase in the cytoplasm. Other PTMs that decrease H1 affinity for chromatin like acetylation or parylation, together with other phosphorylations could also play a role in H1 localization to the cytoplasm (Andrés et al., 2021). However, it is reasonable to think that a part of the H1 in the cytoplasm corresponds to newly synthesized proteins that are not transported to the nucleus.

There are two main pathways to proteasome degradation, ubiquitin-dependent and ubiquitin independent. The ubiquitin-proteasome system controls the metabolism of more than half of the intracellular proteins (Ciechanover A, 2015). This pathway controls the protein levels of some core histone variants in response to EGF stimulation, SIRT1 overexpression, and during mitosis in embryonic cells (Xia et al., 2017; Baptista et al., 2013; Oh et al., 2020). In contrast, the accumulation of H1 subtypes upon proteasome inhibition didn't result in the appearance of high molecular weight bands corresponding to monoubiquitinated or polyubiquitinated H1s. Immunoprecipitation of His-tagged ubiquitin confirmed that the contribution of this proteolytic mechanism to the control of H1 subtypes is almost nonexistent.

Ubiquitin-independent degradation by the proteasome can occur through different mechanisms (Kudriaeva et al., 2019; Fricker LD, 2020). Histone H1 has already been described to be degraded by the 20S proteasome in response to oxidative stress (Ullrich and Grune, 2001; Cervantes-

Laurean et al., 2005). One of the recently described signals for protein targeting to 20S proteasome involves intrinsically disordered regions enriched in basic amino acids (Kudriaeva et al., 2019). We found that 20S proteasome can degrade directly recombinant and endogenous H1 subtypes, as well as its CTD, suggesting that this mechanism could be relevant for H1 targeting and degradation. The analysis of the proteolytic intermediates by mass spectrometry showed that 20S degradation affected both H1 intrinsically disordered domains, first the CTD, followed by the NTD, confirming our hypothesis.

Ub-independent proteasomal degradation can be carried out directly by 20S proteasome aided by 11S or PA200 regulatory caps (Qian et al., 2013, Kudriaeva et al., 2019; Fricker LD, 2020). Degradation by the 20S-PA200 proteasome controls the levels of certain core histone PTMs, while the 11S regulatory cap increases the efficiency of the myelin basic protein degradation (Qian et al., 2013, Kudriaeva et al., 2019). Further experiments are needed to determine whether the regulatory particles 11S or PA200 contribute to target H1 to the 20S proteasome.

In summary, our findings highlight the tight regulation of histone H1 protein levels that involve proteasome degradation and probably transcriptional downregulation. Upon proteasome inhibition, the total amount of H1 within the nucleus remained unchanged, while its excess accumulated in the cytoplasm. The alteration in the subcellular distribution minimized the changes in chromatin structure and transcription that could arise from H1 accumulation within the nucleus. We described, for the first time, that H1 intrinsically disordered CTD acts as a primary determinant for its targeting and degradation by the 20S proteasome.

Funding

This work was supported by grants from the Ministerio de Economía y Competitividad (MINECO) BFU2017-82805-C2-2-P and PID2020-112783GB-C22 awarded to Alicia Roque. Daniel García-Gomis is supported by a PhD fellowship (PIF), awarded by the Autonomous University of Barcelona.

References

Aberle H, Bauer A, Stappert J, Kispert A, Kemler R. Beta-catenin is a target for the ubiquitin-proteasome pathway. EMBO J. 1997 Jul 1;16(13):3797-804. doi: 10.1093/emboj/16.13.3797.

Andrés M, García-Gomis D, Ponte I, Suau P, Roque A. Histone H1 Post-Translational Modifications: Update and Future Perspectives. Int J Mol Sci. 2020 Aug 18;21(16):5941. doi:10.3390/ijms21165941.

Baptista T, Graça I, Sousa EJ, Oliveira AI, Costa NR, Costa-Pinheiro P, Amado F, Henrique R, Jerónimo C. Regulation of histone H2A.Z expression is mediated by sirtuin 1 in prostate cancer. Oncotarget. 2013 Oct;4(10):1673-85. doi: 10.18632/oncotarget.1237.

Bhan S, May W, Warren SL, Sittman DB. Global gene expression analysis reveals specific and redundant roles for H1 variants, H1c and H1(0), in gene expression regulation. Gene. 2008 May 15;414(1-2):10-8. doi: 10.1016/j.gene.2008.01.025.

Bates DL, Thomas JO. Histones H1 and H5: one or two molecules per nucleosome? Nucleic Acids Res. 1981 Nov 25;9(22):5883-94. doi: 10.1093/nar/9.22.5883.

Beacon TH, Davie JR. Transcriptionally Active Chromatin-Lessons Learned from the Chicken Erythrocyte Chromatin Fractionation. Cells. 2021 May 30;10(6):1354. doi: 10.3390/cells10061354.

Bibo-Verdugo B, Jiang Z, Caffrey CR, O'Donoghue AJ. Targeting proteasomes in infectious organisms to combat disease. FEBS J. 2017 May;284(10):1503-1517. doi: 10.1111/febs.14029.

Bleher R, Martin R. Nucleo-cytoplasmic translocation of histone H1 during the HeLa cell cycle. Chromosoma. 1999 Sep;108(5):308-16. doi: 10.1007/s004120050382.

Bolton SJ, Russelakis-Carneiro M, Betmouni S, Perry VH. Non-nuclear histone H1 is upregulated in neurones and astrocytes in prion and Alzheimer's diseases but not in acute neurodegeneration. Neuropathol Appl Neurobiol. 1999 Oct;25(5):425-32. doi: 10.1046/j.1365-2990.1999.00171.x.

Brown DT, Alexander BT, Sittman DB. Differential effect of H1 variant overexpression on cell cycle progression and gene expression. Nucleic Acids Res. 1996 Feb 1;24(3):486-93. doi: 10.1093/nar/24.3.486.

Cerf C, Lippens G, Muyldermans S, Segers A, Ramakrishnan V, Wodak SJ, Hallenga K, Wyns L. Homo- and heteronuclear two-dimensional NMR studies of the globular domain of histone H1: sequential assignment and secondary structure. Biochemistry. 1993 Oct 26;32(42):11345-51. doi: 10.1021/bi00093a011.

Cervantes-Laurean D, Roberts MJ, Jacobson EL, Jacobson MK. Nuclear proteasome activation and degradation of carboxymethylated histones in human keratinocytes following glyoxal treatment. Free Radic Biol Med. 2005 Mar 15;38(6):786-95. doi: 10.1016/j.freeradbiomed.2004.11.030.

Ciechanover A. The unravelling of the ubiquitin system.Nat Rev Mol Cell Biol. 2015 May;16(5):322-4. doi: 10.1038/nrm3982.

Delcuve GP, Davie JR. Chromatin structure of erythroid-specific genes of immature and mature chicken erythrocytes. Biochem J. 1989 Oct 1;263(1):179-86. doi: 10.1042/bj2630179.

Dhaenens M, Glibert P, Meert P, Vossaert L, Deforce D. Histone proteolysis: a proposal for categorization into 'clipping' and 'degradation'. Bioessays. 2015 Jan;37(1):70-9. doi: 10.1002/bies.201400118.

Di Liegro CM, Schiera G, Di Liegro I. H1.0 Linker Histone as an Epigenetic Regulator of Cell Proliferation and Differentiation. Genes (Basel). 2018 Jun 20;9(6):310. doi: 10.3390/genes9060310.

Duerre JA, Lee CT. In vivo methylation and turnover of rat brain histones. J Neurochem. 1974 Sep;23(3):541-7. doi: 10.1111/j.1471-4159.1974.tb06057.x.

Duronio RJ, Marzluff WF. Coordinating cell cycle-regulated histone gene expression through assembly and function of the Histone Locus Body. RNA Biol. 2017 Jun 3;14(6):726-738. doi: 10.1080/15476286.2016.1265198.

Goytisolo,F.A., Gerchman,S.E., Yu,X., Rees,C., Graciano,V., Ramakrishnan,V. and Thomas,J.O. (1996) Identification of two DNA binding sites on the globular domain of histone H5. EMBO J., 15, 3421–3429.

Gunjan A, Alexander BT, Sittman DB, Brown DT. Effects of H1 histone variant overexpression on chromatin structure. J Biol Chem. 1999 Dec 31;274(53):37950-6. doi: 10.1074/jbc.274.53.37950.

Fan Y, Nikitina T, Morin-Kensicki EM, Zhao J, Magnuson TR, Woodcock CL, Skoultchi AI. H1 linker histones are essential for mouse development and affect nucleosome spacing in vivo. Mol Cell Biol. 2003 Jul;23(13):4559-72. doi: 10.1128/MCB.23.13.4559-4572.2003.

Fan Y, Nikitina T, Zhao J, Fleury TJ, Bhattacharyya R, et al. Histone H1 depletion in mammals alters global chromatin structure but causes specific changes in gene regulation. Cell. 2005;123:1199–1212. doi: 10.1016/j.cell.2005.10.028.

Fricker LD. Proteasome Inhibitor Drugs. Annu. Rev. Pharmacol. Toxicol. 2020. 60:457–76. doi: 10.1146/annurev-pharmtox-010919-023603.

Goldberg AL. Development of proteasome inhibitors as research tools and cancer drugs. J Cell Biol. 2012 Nov 12;199(4):583-8. doi: 10.1083/jcb.201210077.

Hansen JC, Lu X, Ross ED, Woody RW. Intrinsic protein disorder, amino acid composition, and histone terminal domains. J Biol Chem 2006, 281:1853–1856. doi: 10.1074/jbc.R500022200.

Harshman SW, Chen MM, Branson OE, Jacob NK, Johnson AJ, Byrd JC, Freitas MA. Isolation and analysis of linker histones across cellular compartments. J Proteomics. 2013 Oct 8;91:595-604. doi: 10.1016/j.jprot.2013.08.022.

Hendzel MJ, Lever MA, Crawford E, Th'ng JP. The C-terminal domain is the primary determinant of histone H1 binding to chromatin in vivo. J Biol Chem. 2004 May 7;279(19):20028-34. doi: 10.1074/jbc.M400070200.

Izquierdo-Bouldstridge A, Bustillos A, Bonet-Costa C, Aribau-Miralbés P, García-Gomis D, Dabad M, Esteve-Codina A, Pascual-Reguant L, Peiró S, Esteller M, Murtha M, Millán-Ariño L, Jordan A. Histone H1 depletion triggers an interferon response in cancer cells via activation of

heterochromatic repeats. Nucleic Acids Res. 2017 Nov 16;45(20):11622-11642. doi: 10.1093/nar/gkx746.

Kisselev AF, van der Linden WA, Overkleeft HS. Proteasome inhibitors: an expanding army attacking a unique target. Chem Biol. 2012 Jan 27;19(1):99-115. doi: 10.1016/j.chembiol.2012.01.003.

Kudriaeva A, Kuzina ES, Zubenko O, Smirnov IV, Belogurov A Jr. Charge-mediated proteasome targeting. FASEB J. 2019 Jun;33(6):6852-6866. doi: 10.1096/fj.201802237R.

Kwon M, Firestein BL. DNA transfection: calcium phosphate method Methods Mol Biol. 2013;1018:107-10. doi: 10.1007/978-1-62703-444-9_10.

Leicher R, Osunsade A, Chua GNL, Faulkner SC, Latham AP, Watters JW, Nguyen T, Beckwitt EC, Christodoulou-Rubalcava S, Young PG, Zhang B, David Y, Liu S. Single-stranded nucleic acid binding and coacervation by linker histone H1. Nat Struct Mol Biol. 2022 May;29(5):463-471. doi: 10.1038/s41594-022-00760-4.

Livak KJ, Schmittgen TD. Analysis of relative gene expression data using real-time quantitative PCR and the 2(-Delta Delta C(T)) Method. Methods. 2001 Dec;25(4):402-8. doi: 10.1006/meth.2001.1262.

Lopez R, Sarg B, Lindner H, Bartolomé S, Ponte I, Suau P, Roque A. Linker histone partial phosphorylation: effects on secondary structure and chromatin condensation. Nucleic Acids Res. 2015 May 19;43(9):4463-76. doi: 10.1093/nar/gkv304.

McConkey DJ. Calcium-dependent, interleukin 1-converting enzyme inhibitor-insensitive degradation of lamin B1 and DNA fragmentation in isolated thymocyte nuclei. J Biol Chem. 1996 Sep 13;271(37):22398-406. doi: 10.1074/jbc.271.37.22398.

Millán-Ariño L, Izquierdo-Bouldstridge A, Jordan A. Specificities and genomic distribution of somatic mammalian histone H1 subtypes. Biochim Biophys Acta. 2016 Mar;1859(3):510-9. doi: 10.1016/j.bbagrm.2015.10.013.

Murakami Y, Matsufuji S, Kameji T, Hayashi S, Igarashi K, Tamura T, Tanaka K, Ichihara A. Ornithine decarboxylase is degraded by the 26S proteasome without ubiquitination. Nature. 1992 Dec 10;360(6404):597-9. doi: 10.1038/360597a0.

Oh E, Mark KG, Mocciaro A, Watson ER, Prabu JR, Cha DD, Kampmann M, Gamarra N, Zhou CY, Rape M. Gene expression and cell identity controlled by anaphase-promoting complex. Nature. 2020 Mar;579(7797):136-140. doi: 10.1038/s41586-020-2034-1.

Pan C, Fan Y. Role of H1 linker histones in mammalian development and stem cell differentiation. Biochim Biophys Acta. 2016 Mar;1859(3):496-509. doi: 10.1016/j.bbagrm.2015.12.002

Peters JM, Franke WW, Kleinschmidt JA. Distinct 19 S and 20 S subcomplexes of the 26 S proteasome and their distribution in the nucleus and the cytoplasm. J Biol Chem. 1994 Mar 11;269(10):7709-18.

Ponte I, Vidal-Taboada JM, Suau P. Evolution of the vertebrate H1 histone class: evidence for the functional differentiation of the subtypes. Mol Biol Evol. 1998 Jun;15(6):702-8. doi: 10.1093/oxfordjournals.molbev.a025973.

Ponte I, Andrés M, Jordan A, Roque A. Towards understanding the Regulation of Histone H1 Somatic Subtypes with OMICs. J Mol Biol. 2021 Jan 22;433(2):166734. doi: 10.1016/j.jmb.2020.166734.

Qian MX, Pang Y, Liu CH, Haratake K, Du BY, Ji DY, et al. Acetylation-mediated proteasomal degradation of core histones during DNA repair and spermatogenesis. Cell. 2013 May 23;153(5):1012-24. doi: 10.1016/j.cell.2013.04.032.

Raghuram N, Strickfaden H, McDonald D, Williams K, Fang H, Mizzen C, Hayes JJ, Th'ng J, Hendzel MJ: Pin1 promotes histone H1 dephosphorylation and stabilizes its binding to chromatin. J Cell Biol 2013, 203:57–71. doi: 10.1083/jcb.201305159.

Ramakrishnan V, Finch JT, Graziano V, Lee PL, Sweet RM. Crystal structure of globular domain of histone H5 and its implications for nucleosome binding. Nature. 1993 Mar 18;362(6417):219-23. doi: 10.1038/362219a0.

Roque A, Orrego M, Ponte I, Suau P. The preferential binding of histone H1 to DNA scaffold-associated regions is determined by its C-terminal domain. Nucleic Acids Research 2004. 32 (20), 6111-6119. doi: 10.1093/nar/gkh945.

Roque A, Iloro I, Ponte I, Arrondo JL, Suau P. DNA-induced secondary structure of the carboxyl-terminal domain of histone H1. J Biol Chem. 2005 Sep 16;280(37):32141-7. doi: 10.1074/jbc.M505636200.

Roque A, Ponte I, Arrondo JL, Suau P. Phosphorylation of the carboxy-terminal domain of histone H1: effects on secondary structure and DNA condensation. Nucleic Acids Res. 2008 Aug;36(14):4719-26. doi: 10.1093/nar/gkn440.

Shabek N, Herman-Bachinsky Y, Buchsbaum S, Lewinson O, Haj-Yahya M, Hejjaoui M, Lashuel HA, Sommer T, Brik A, Ciechanover A. The size of the proteasomal substrate determines whether its degradation will be mediated by mono- or polyubiquitylation. Mol Cell. 2012 Oct 12;48(1):87-97. doi: 10.1016/j.molcel.2012.07.011.

Shmueli MD, Sheban D, Eisenberg-Lerner A, Merbl Y. Histone degradation by the proteasome regulates chromatin and cellular plasticity. FEBS J. 2022 Jun;289(12):3304-3316. doi: 10.1111/febs.15903.

Singh RK, Liang D, Gajjalaiahvari UR, Kabbaj MH, Paik J, Gunjan A. Excess histone levels mediate cytotoxicity via multiple mechanisms. Cell Cycle. 2010 Oct 15;9(20):4236-44. doi: 10.4161/cc.9.20.13636.

Talbert PB, Ahmad K, Almouzni G, Ausió J, Berger F, Bhalla PL, et al. A unified phylogeny-based nomenclature for histone variants. Epigenetics Chromatin. 2012 Jun 21;5:7. doi: 10.1186/1756-8935-5-7.

Ullrich O, Grune T. Proteasomal degradation of oxidatively damaged endogenous histones in K562 human leukemic cells. Free Radic Biol Med. 2001 Oct 1;31(7):887-93. doi: 10.1016/s0891-5849(01)00672-4.

Vila R, Ponte I, Collado M, Arrondo JL, Jiménez MA, Rico M, Suau P. DNA-induced alpha-helical structure in the NH2-terminal domain of histone H1. J Biol Chem. 2001 Dec 7;276(49):46429-35. doi: 10.1074/jbc.M106952200.

Vila R, Ponte I, Jiménez MA, Rico M, Suau P. An inducible helix-Gly-Gly-helix motif in the N-terminal domain of histone H1e: a CD and NMR study. Protein Sci. 2002 Feb;11(2):214-20. doi: 10.1110/ps.29602.

Voelkel-Johnson C, Entingh AJ, Wold WS, Gooding LR, Laster SM. Activation of intracellular proteases is an early event in TNF-induced apoptosis. J Immunol. 1995 Feb 15;154(4):1707-16. 4159.2007.04637.x. PMID: 17504267.

Xia Y, Yang W, Fa M, Li X, Wang Y, Jiang Y, Zheng Y, Lee JH, Li J, Lu Z. RNF8 mediates histone H3 ubiquitylation and promotes glycolysis and tumorigenesis. J Exp Med. 2017 Jun 5;214(6):1843-1855. doi: 10.1084/jem.20170015.

Zafar KS, Inayat-Hussain SH, Ross D. A comparative study of proteasomal inhibition and apoptosis induced in N27 mesencephalic cells by dopamine and MG132. J Neurochem. 2007 Aug;102(3):913-21. doi: 10.1111/j.1471.

Zhang Y, Cooke M, Panjwani S, Cao K, Krauth B, Ho PY, Medrzycki M, Berhe DT, Pan C, McDevitt TC, Fan Y. Histone h1 depletion impairs embryonic stem cell differentiation. PLoS Genet. 2012;8(5):e1002691. doi: 10.1371/journal.pgen.1002691.

Zlatanova JS, Srebreva LN, Banchev TB, Tasheva BT, Tsanev RG. Cytoplasmic pool of histone H1 in mammalian cells. J Cell Sci. 1990 Jul;96 (Pt 3):461-8. doi: 10.1242/jcs.96.3.461.

Figure captions.

Figure 1: Effects of proteasome inhibition on Histone H1 variants in T47D cells. A. Western Blots of total protein extracts of T47D cells treated with DMSO, MG132 (20µM 12h), and Bortezomib (20nM 12h). C. Western Blots of total protein extract after translation inhibition treatment by cycloheximide (10 µg/ml 8h). B, D. Quantification of the Western blot images of several biological replicates corresponding to A and C, respectively. E. Scatter plot and correlation between protein accumulation and protein stability.

Figure 2: Accumulation of histone H1 subtypes in the cytoplasm of T47D cells after proteasome inhibition with MG132. A. Representative immunohistochemistry images of histone H1 somatic subtypes on T47D cells. The cell nucleus was stained with DAPI. B. Box plots correspond to the quantification of 35-70 cells/subtype and condition. Asterisks denote the p-value of the two-tailed Student's t-test showing the significance of the difference between untreated and treated cells * p-value < 0.05; ** p-value < 0.01; *** p-value < 0.001; n.s, not significant.

Figure 3. Accumulation of histone H1p and H1T46p in the cytoplasm of T47D cells after proteasome inhibition with MG132. A. Representative immunohistochemistry images of H1p and H1T56p on T47D cells. Cells were treated with DMSO and MG132 (20 µM 12h). The cell nucleus was stained with DAPI. B. Box plots correspond to the quantification of 35-70 cells/modification and condition. Asterisks denote the p-value of the two-tailed Student's t-test showing the significance of the difference between untreated and treated cells * p-value < 0.05; ** p-value < 0.01.

Figure 4: Effects of the accumulation of histone H1 subtypes in chromatin. A. Western Blots and quantification of chromatin-bound H1. B. Quantification of the Western blot images. C. SDS-PAGE of total histone extractions from whole cells and isolated nuclei. D. Fold change of the H1: nucleosome ratio between MG132 and DMSO in whole cells and nuclear extracts. E. Digestion with micrococcal nuclease of chromatin of cells treated with DMSO and MG132. F. Nucleosome repeat length calculated from the digestions shown in E. In all the experiments cells were treated with DMSO as a negative control or with MG132 (20µM 12h).

Figure 5. Contribution of the ubiquitin-dependent pathway to H1 degradation. Effects of proteasome inhibition in HEK293T cells. A. Western Blot of total protein extracts upon proteasome inhibition with MG132 (20µM 12h). B. Quantification of the Western blot images of several biological replicates. C. WB of Immunoprecipitation of HEK293T cells carrying a tagged ubiquitin and treated with or without MG132.

Figure 6: **Histone H1 degradation by the 20S proteasome.** A. Silver staining of in vitro degradation of purified proteins with the 20S proteasome. H1.0, its C-terminal domain (CTD), and its globular domain (GD) are recombinant proteins. Native H1s were obtained by perchloric extraction of T47D cells nuclei. BSA was used as a negative control. B. Proteoforms of recombinant H1.0 identified by top-down mass spectrometry after digestion with the 20S proteasome.

Figure 1.

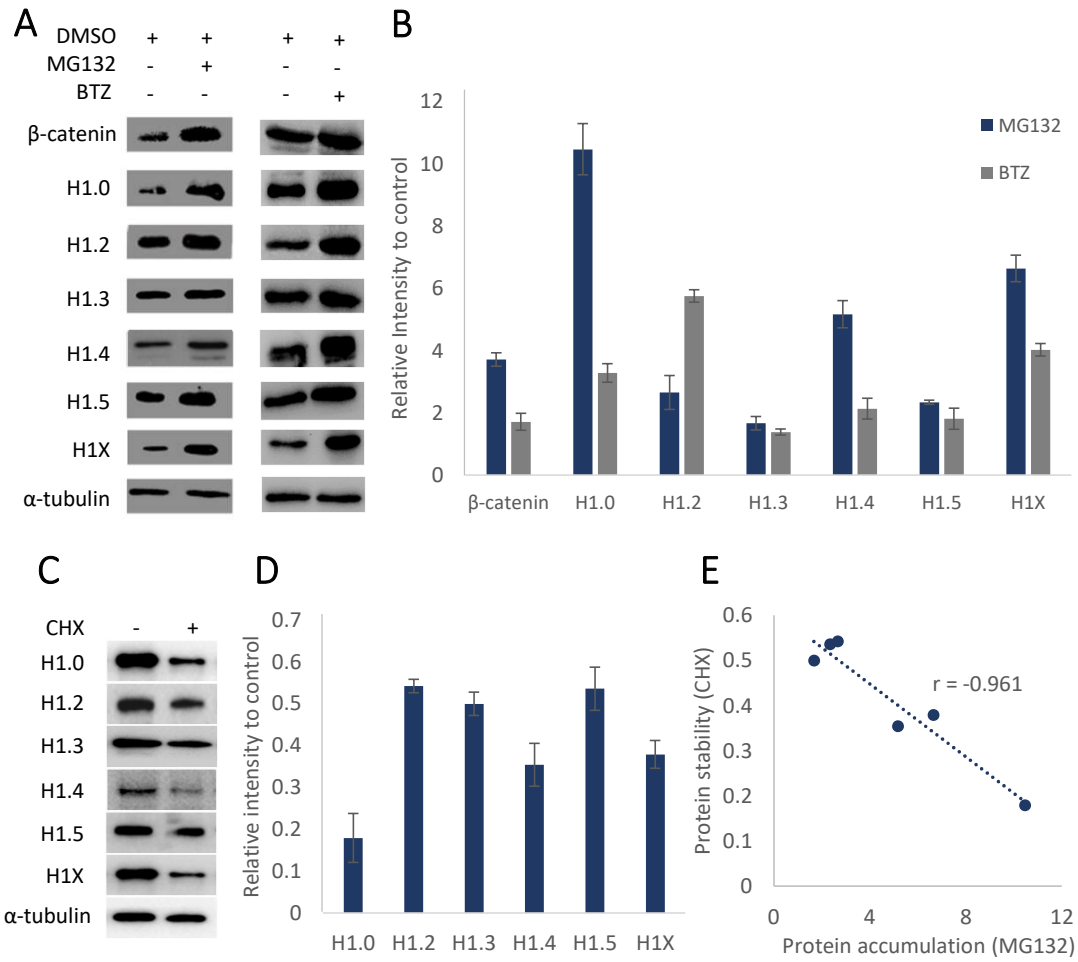
A
DMSO + + + +
MG132 - + - -
BTZ - - - +
β-catenin
H1.0
H1.2
H1.3
H1.4
H1.5
H1X
α-tubulin
B
Relative Intensity to control
12
10
8
6
4
2
0
MG132
BTZ
β-catenin H1.0 H1.2 H1.3 H1.4 H1.5 H1X
C
CHX - +
H1.0
H1.2
H1.3
H1.4
H1.5
H1X
α-tubulin
D
Relative intensity to control
0.7
0.6
0.5
0.4
0.3
0.2
0.1
0
H1.0 H1.2 H1.3 H1.4 H1.5 H1X
E
Protein stability (CHX)
0.6
0.5
0.4
0.3
0.2
0.1
0
r = -0.961
0 4 8 12
Protein accumulation (MG132)

Figure 2.

A

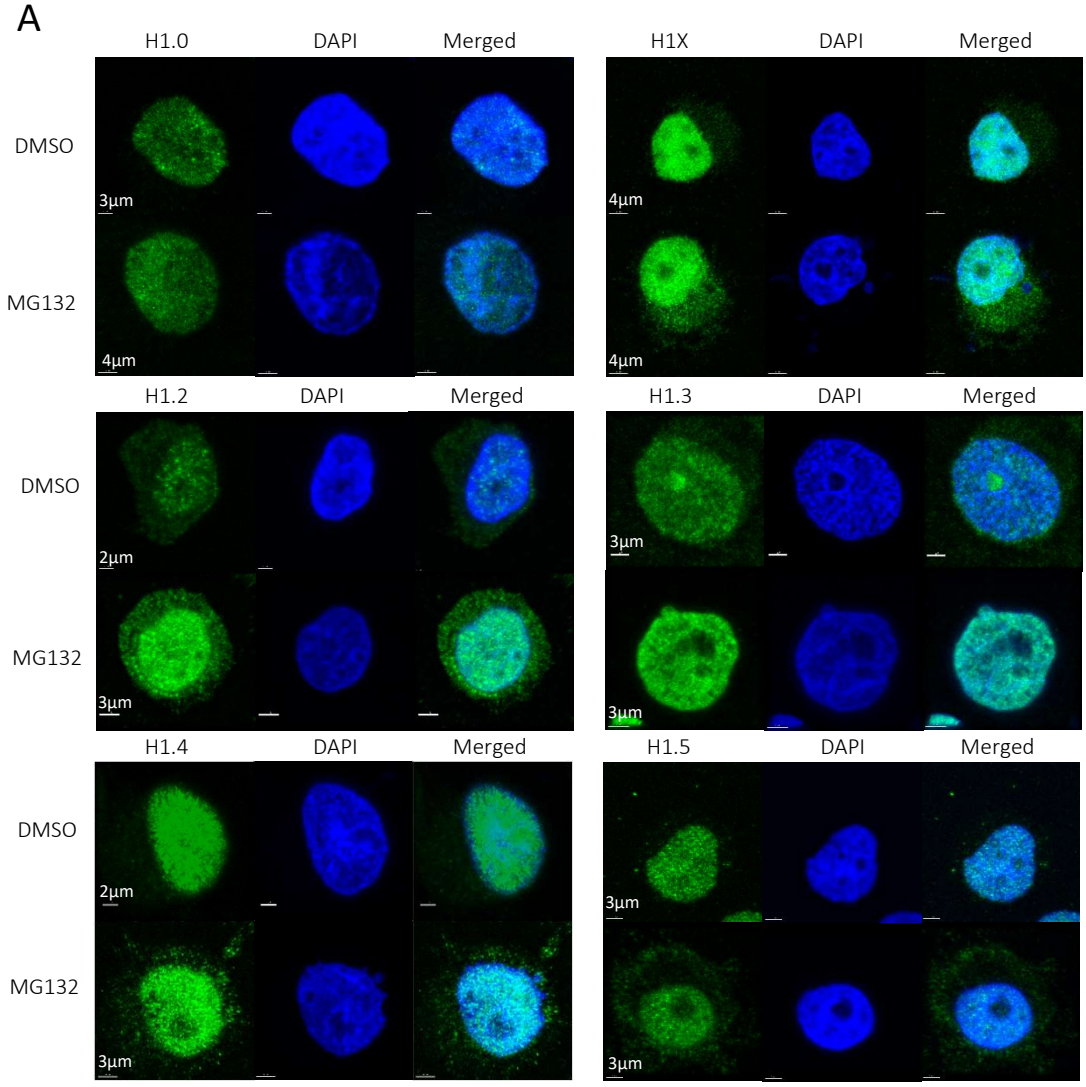
H1.0
DAPI
Merged
H1X
DAPI
Merged
DMSO
MG132
3µm
4µm
4µm
4µm
H1.2
DAPI
Merged
H1.3
DAPI
Merged
DMSO
MG132
2µm
3µm
3µm
3µm
H1.4
DAPI
Merged
H1.5
DAPI
Merged
DMSO
MG132
2µm
3µm
3µm
3µm

B

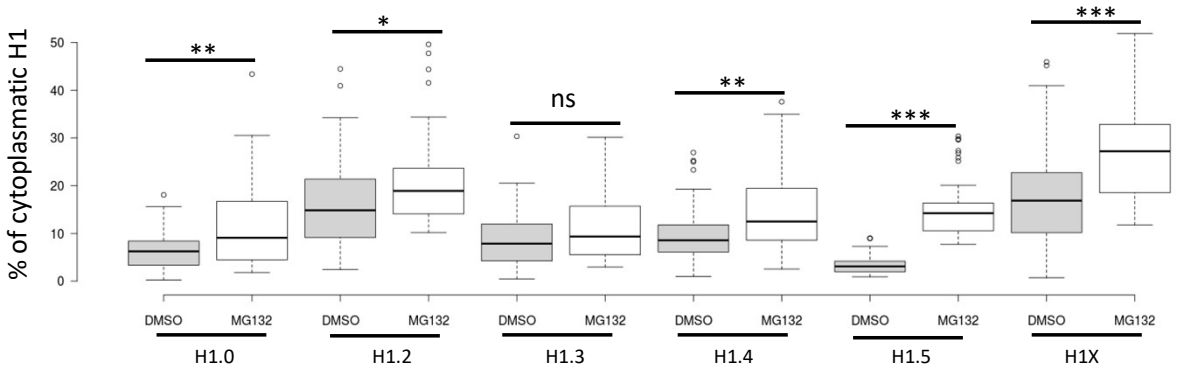
% of cytoplasmatic H1
50
40
30
20
10
0
**
*
ns
**
***
***
DMSO
MG132
H1.0
H1.2
H1.3
H1.4
H1.5
H1X

Figure 3.

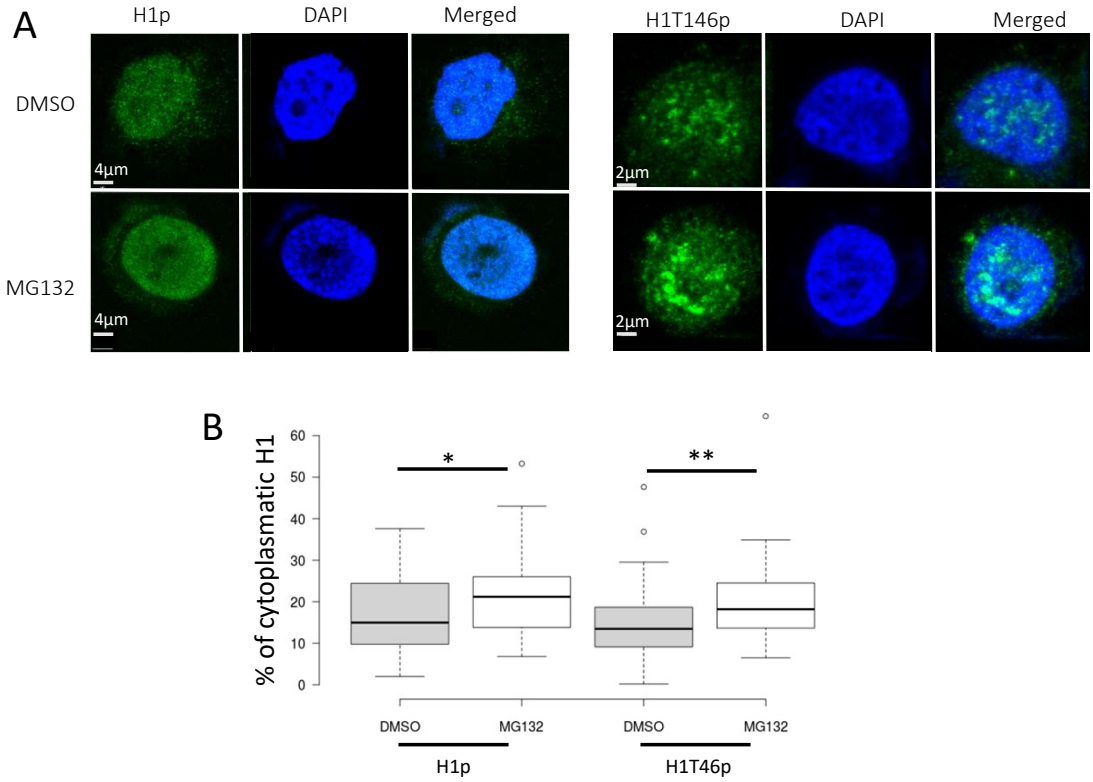
A
H1p
DAPI
Merged
H1T146p
DAPI
Merged
DMSO
MG132
4µm
4µm
2µm
2µm
B
% of cytoplasmatic H1
60
50
40
30
20
10
0
*
**
DMSO
MG132
DMSO
MG132
H1p
H1T46p

Figure 4.

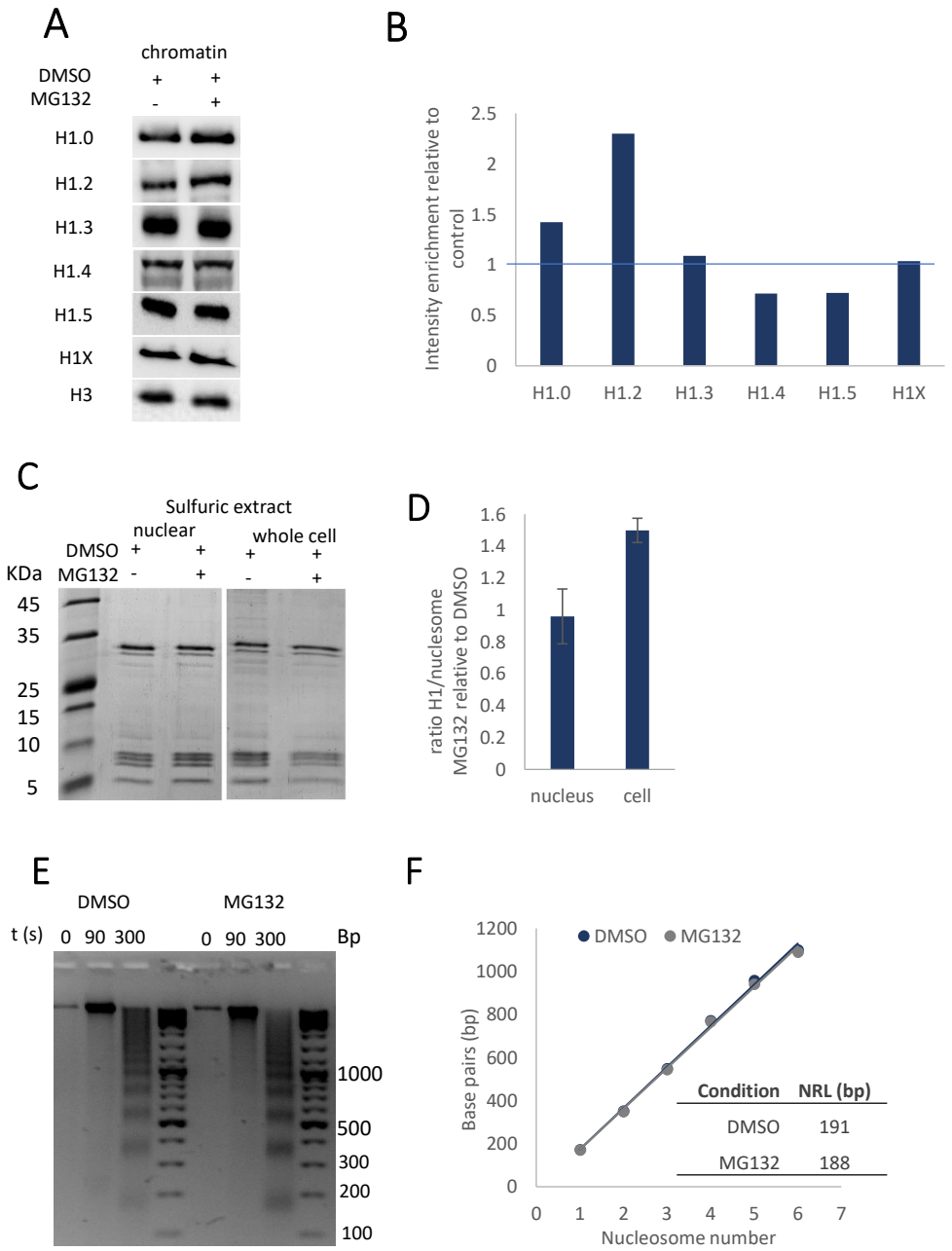
A
chromatin
DMSO + +
MG132 - +
H1.0
H1.2
H1.3
H1.4
H1.5
H1X
H3
B
Intensity enrichment relative to control
2.5
2
1.5
1
0.5
0
H1.0
H1.2
H1.3
H1.4
H1.5
H1X
C
Sulfuric extract
nuclear
whole cell
DMSO + + + +
KDa MG132 - + - +
45
35
25
15
10
5
D
ratio H1/nucleosome MG132 relative to DMSO
1.6
1.4
1.2
1
0.8
0.6
0.4
0.2
0
nucleus
cell
E
DMSO
MG132
t (s) 0 90 300 0 90 300 Bp
1000
500
300
200
100
F
DMSO
MG132
Base pairs (bp)
1200
1000
800
600
400
200
0
0 1 2 3 4 5 6 7
Nucleosome number
Condition NRL (bp)
DMSO 191
MG132 188

Figure 5.

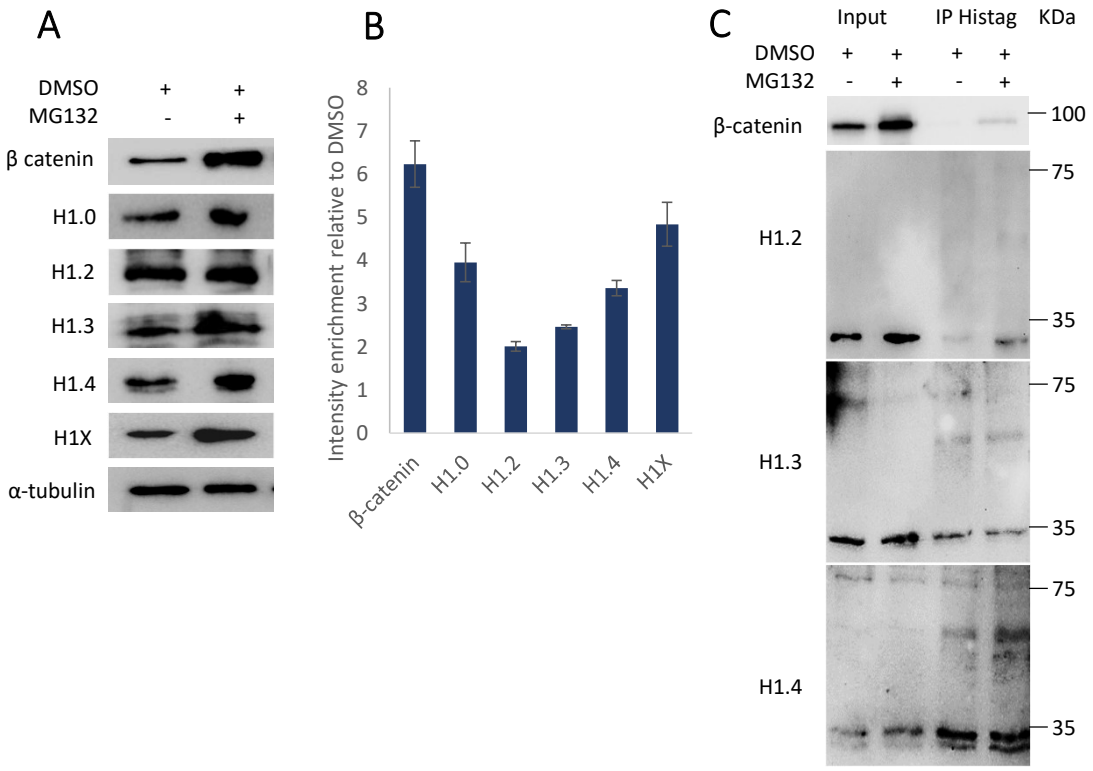
A
DMSO + +
MG132 - +
β catenin
H1.0
H1.2
H1.3
H1.4
H1X
α-tubulin
B
Intensity enrichment relative to DMSO
0
1
2
3
4
5
6
7
8
β-catenin
H1.0
H1.2
H1.3
H1.4
H1X
C
Input
IP Histag
KDa
DMSO + + + +
MG132 - + - +
β-catenin
H1.2
H1.3
H1.4
100
75
35
75
35
75
35

Figure 6.

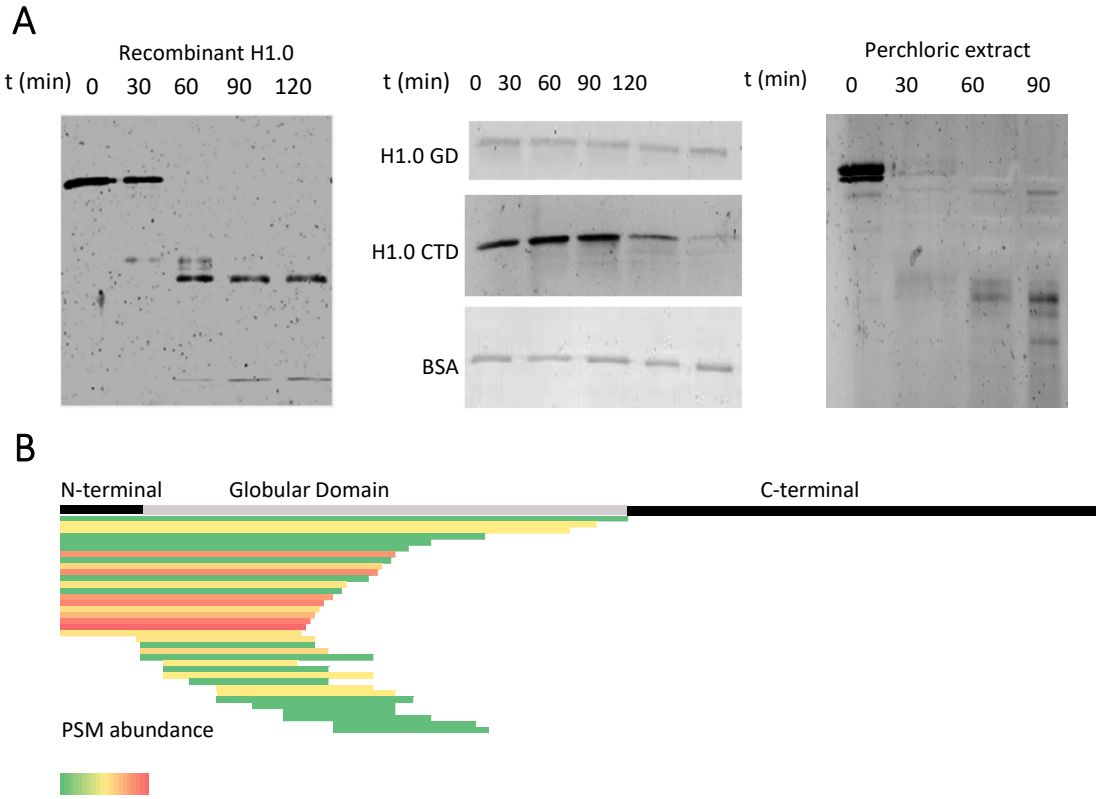
A
Recombinant H1.0
t (min) 0 30 60 90 120
t (min) 0 30 60 90 120
H1.0 GD
H1.0 CTD
BSA
Perchloric extract
t (min) 0 30 60 90
B
N-terminal
Globular Domain
C-terminal
PSM abundance